journal of the mechanical behavior of biomedical materials 112 (2020) 104038

Contents lists available at ScienceDirect

Journal of the Mechanical Behavior of Biomedical Materials

journal homepage: www.elsevier.com/locate/jmbbm

Research paper

Hyperelastic and viscoelastic characterization of hepatic tissue under uniaxial tension in time and frequency domain

Sarah-Jane Estermann [a,b,c], Dieter H. Pahr [a,c], Andreas Reisinger [a,*]

[a] Department Anatomy and Biomechanics, Karl Landsteiner University of Health Sciences, Dr.-Karl-Dorrek-Straße 30, 3500 Krems an der Donau, Austria
[b] Austrian Center for Medical Innovation and Technology, Viktor Kaplan-Straße 2/1, 2700 Wiener Neustadt, Austria
[c] Institute for Lightweight Design and Structural Biomechanics, TU-Wien, Getreidemarkt 9, 1060 Wien, Austria

ARTICLE INFO

Keywords:
Hepatic tissue
Tensile testing
Viscoelasticity
Hyperelasticity
Stress relaxation
Dynamic mechanical analysis

ABSTRACT

In order to create accurate anatomical models for medical training and research, mechanical properties of biological tissues need to be studied. However, non-linear and viscoelastic behaviour of most soft biological tissues complicates the evaluation of their mechanical properties. In the current study, a method for measuring hyperelasticity and viscoelasticity of bovine and porcine hepatic parenchyma in tension is presented.

First, non-linear stress–stretch curves resulting from ramp loading and unloading, were interpreted based on a hyperelastic framework, using a Veronda–Westmann strain energy function. Strain-specific elastic moduli, such as initial stiffness E_I, were thereupon defined in certain parts of the stress–stretch curves. Furthermore, dissipated and stored energy density were calculated. Next, the viscoelastic nature of liver tissue was examined with two different methods: stress relaxation and dynamic cyclic testing. Both tests yielded dissipated and stored energy density, as well as loss tangent ($\tan\delta$), storage modulus (E'), and loss modulus (E''). In tension, stress relaxation was experimentally more convenient than dynamic cyclic testing. Thus we considered whether relaxation could be used for approximating the results of the cyclic tests.

Regarding the resulting elastic moduli, initial stiffness was similar for porcine and bovine liver ($E_I \sim 30$ kPa), while porcine liver was stiffer for higher strains. Comparing stress relaxation with dynamic cyclic testing, $\tan\delta$ of porcine and bovine liver was the same for both methods ($\tan\delta = 0.05 - 0.25$ at 1 Hz). Storage and loss moduli matched well for bovine, but not as well for porcine tissue.

In conclusion, the utilized Veronda–Westmann model was appropriate for representing the hyperelasticity of liver tissue seen in ramp tests. Concerning viscoelasticity, both chosen testing methods – stress relaxation and dynamic cyclic testing – yielded comparable results for E', E'', and $\tan\delta$, as long as elasticity non-linearities were heeded.

The here presented method provides novel insight into the tensile viscoelastic properties of hepatic tissue, and provides guidelines for convenient evaluation of soft tissue mechanical properties.

1. Introduction

Surgical training requires scenarios that are as life-like as possible. However, before practising on real *in vivo* patients, teaching models are necessary. The use of fresh human tissue is limited due to ethical concerns, availability, and safety issues. Thus, models usually consist of preserved human cadavers, animal organs or artificial materials.

Especially, the increasing trend towards minimally invasive methods in general surgery calls for improved laparoscopic training systems (Alli et al., 2017; Armijo et al., 2018; Chen et al., 2020). Cholecystectomy and hepatectomy, for instance, are common surgical procedures that are widely being performed laparoscopically and require corresponding training systems which must include the liver (Alli et al., 2017; Yoshida et al., 2019). In this context, porcine and bovine liver models are deemed useful for laparoscopic training (Hildebrand et al., 2007; Laird et al., 2011; Liu et al., 2018). Furthermore, liver models are important for risk analysis in crash tests, due to the high susceptibility of the liver to injury during vehicular crashes (Yoganandan et al., 2000; Kemper et al., 2010). Another application for hepatic models is in practising palpation to distinguish fibrotic from healthy tissue and identifying tumours in open surgery approaches (Hata et al., 2011). It is therefore important to accurately measure liver mechanical properties in order to manufacture realistic models.

In general, characterizing mechanical properties of soft tissue can be challenging due to potentially non-linear and viscoelastic material

* Corresponding author.
E-mail address: andreas.reisinger@kl.ac.at (A. Reisinger).

https://doi.org/10.1016/j.jmbbm.2020.104038
Received 29 May 2020; Received in revised form 3 August 2020; Accepted 10 August 2020
Available online 24 August 2020

behaviour, as well as the need for measuring small loads resulting from the low stiffness (with the Young's modulus typically ~1 MPa (Akhtar et al., 2011)).

Hepatic tissue is difficult to handle in experimental setups and has predominantly been studied in compression (Tamura et al., 2002; Kiss et al., 2004; Ocal et al., 2010; DeWall et al., 2012; Jing et al., 2016) and shear (Liu and Bilston, 2002; Nicolle et al., 2010; Wex et al., 2013; Zhu et al., 2013; Capilnasiu et al., 2020), regarding elastic as well as viscoelastic tissue properties. Tensile tests on hepatic parenchyma have been conducted for evaluating failure properties (Brunon et al., 2010; Kemper et al., 2010; Lu et al., 2014; Duong et al., 2015; Dunford et al., 2018); thus, illuminating the effect of large strains (> 10% (Marchesseau et al., 2017)) on the tissue, as experienced in the context of trauma. However, it is also interesting to study liver under small strains relevant for tactile properties.

Ramp tests of hepatic tissue result in non-linear stress–strain curves (Chen et al., 1996), suggesting the use of hyperelastic modelling (Chui et al., 2004; Gao et al., 2010; Umale et al., 2013). However, a purely hyperelastic approach neglects viscoelastic behaviour which plays an important role in liver tissue (Liu and Bilston, 2000). As a partial solution to this problem, the idea of pseudoelasticity was introduced by Fung (1993) for interpreting loading–unloading curves exhibiting hysteresis (which is an indicator for viscoelasticity), utilizing a hyperelastic framework: Loading and unloading is thereby modelled separately, yielding two distinct stets of hyperelastic parameters. Another approach to analysing non-linear behaviour is to define certain strain ranges, where elastic moduli can be calculated (Fung, 1967). For example, characteristic low-strain and high-strain elastic moduli were determined for liver capsule (Hollenstein et al., 2006; Karimi and Shojaei, 2018) and for kidney capsule (Snedeker et al., 2005) in uniaxial tension.

However, these methods are only descriptive of what is observed but fail to describe the constitutive effect of viscoelasticity itself. To study viscoelasticity in a more rigorous manner, the most common methods are: testing at different strain rates, stress relaxation (under constant strain), creep (under constant stress), and dynamic cyclic testing (oscillating stress and strain) which is also known as dynamic mechanical analysis (DMA). The results of these various testing methods can be compared with each other. For example, Bartolini et al. (2018) compared viscoelastic properties from indentation at different oscillatory frequencies with indentation at different strain rates for a soft silicone polymer — thus connecting frequency domain and time domain experimental data. Following this train of thought, viscoelastic properties extracted from relaxation experiments could be compared with the same type of properties found in dynamic cyclic tests.

Regarding stress relaxation of hepatic tissue, experiments have been conducted under compression (Taylor et al., 2002), shear (Liu and Bilston, 2000, 2002), tension (Chen et al., 2011) and indentation (Mattice et al., 2006; Estermann et al., 2020). DMA has been done on liver tissue in compressive and shear conditions (Kiss et al., 2004; Capilnasiu et al., 2020). However, the authors are not aware of publications on liver parenchyma exposed to tensile oscillatory strain for assessing tissue viscoelastic properties. This may be due to experimental difficulties connected to tensile testing of extremely soft materials; with DMA being more complex than other testing methods, such as stress relaxation or creep. Thus, the question arises whether simple relaxation data could be utilized instead of DMA for hepatic tissue in tension. Viscoelastic properties, which are usually extracted directly from dynamic cyclic tests (e.g. loss tangent, storage modulus, and loss modulus), can be calculated based on relaxation data via transformation from time domain to frequency domain (Ocal et al., 2010).

The current study aims at a comprehensive characterization of hepatic tensile mechanical properties, meaning that non-linear as well as viscoelastic behaviour must be taken into account. For this reason, different types of tests were conducted on porcine and bovine hepatic parenchyma tissue. First, ramp loading and unloading was done, yielding hysteresis and non-linear behaviour. These curves were interpreted with a pseudoelastic model and elastic moduli, defined at specific strain levels, were calculated. Furthermore, based on energy considerations, the ratio of dissipated to stored energy density was evaluated.

Next, two different methods of viscoelastic characterization – stress relaxation and DMA – were utilized for extracting loss tangent ($\tan\delta$), storage modulus (E'), and loss modulus (E''). These properties stemming from the two testing methods were finally compared with each other, addressing the question whether a simplified viscoelastic evaluation via stress relaxation (assuming an ideal step-displacement) is justified for hepatic tissue in tension. In addition to the above mentioned viscoelastic properties, dissipated and stored energy density were calculated for relaxation and DMA, yielding results that are specific for each testing method.

2. Materials and methods

2.1. Tensile test specimen

Hepatic samples were taken from eight porcine, and two bovine livers, obtained from a local butchery about 24 h after slaughtering and prepared for testing immediately upon arrival in the laboratory (Fig. 1a and b). Between slaughtering and sample preparation, whole livers were stored at ~4 °C in sealed plastic bags. Dunford et al. (2018) recommended storage of liver in large blocks as opposed to small cut samples. Rectangular tensile test specimen were extracted with their long axis orientated parallel to the diaphragmatic and the visceral surface of the organs: First a rectangular block (measuring around 75 × 50 × 30 mm) was cut out of a relatively homogeneous region of the liver (Fig. 1c). After removing the capsule, the block was placed in a 5 mm thick 3D printed cutting guide and a long knife was used for extracting thin rectangular slices by cutting parallel to the guide (Fig. 1d). Next, a 75 × 20 mm stencil was placed on the liver slice and samples were obtained by cutting around the stencil (Fig. 1e). The resulting samples consisted of parenchyma tissue without the Glisson's capsule, free of large blood vessels and bile ducts to ensure relative homogeneity (Fig. 1f). Sample thickness was chosen as ~5 mm due to the fact that samples of under 2.5 mm thickness exhibited dehydration at the sand paper contact area when being clamped in the mechanical testing machine, while significantly thicker samples were difficult to mount and clamp. The total numbers of porcine samples was $n = 36$, as was for the bovine samples whose total number was also $n = 36$. All samples were kept well hydrated by submerging them in 0.9% saline solution. Mechanical testing was conducted immediately after sample preparation at room temperature (~23 °C), thus the tissues were never frozen.

2.2. Mechanical testing

Tensile testing was conducted on a ZwickiLine testing machine (ZwickRoell GmbH & Co. KG, Ulm, Germany) which allows axial forces F up to 2.5 kN and a machine displacement u_M of up to 113 cm. In soft tissue testing, the resulting forces are very small and thus an additional load cell for measuring F, with a measuring range up to 100 N and accuracy of 0.02% (S2M/100N, Hottinger Baldwin Messtechnik GmbH, Darmstadt, Germany) was connected to the universal data acquisition module (DAQ) QuantumX MX840B (Hottinger Baldwin Messtechnik GmbH, Darmstadt, Germany). The load cell was gripped by the lower machine clamp.

Custom-built tissue clamps enabled manual fine-tuning of the gripping force with a screw. One tissue clamp was secured in the upper machine clamp and the other one inserted above the external load cell. The tissue clamping surface was covered with sand paper (grit P80) to prevent sample slippage during tension.

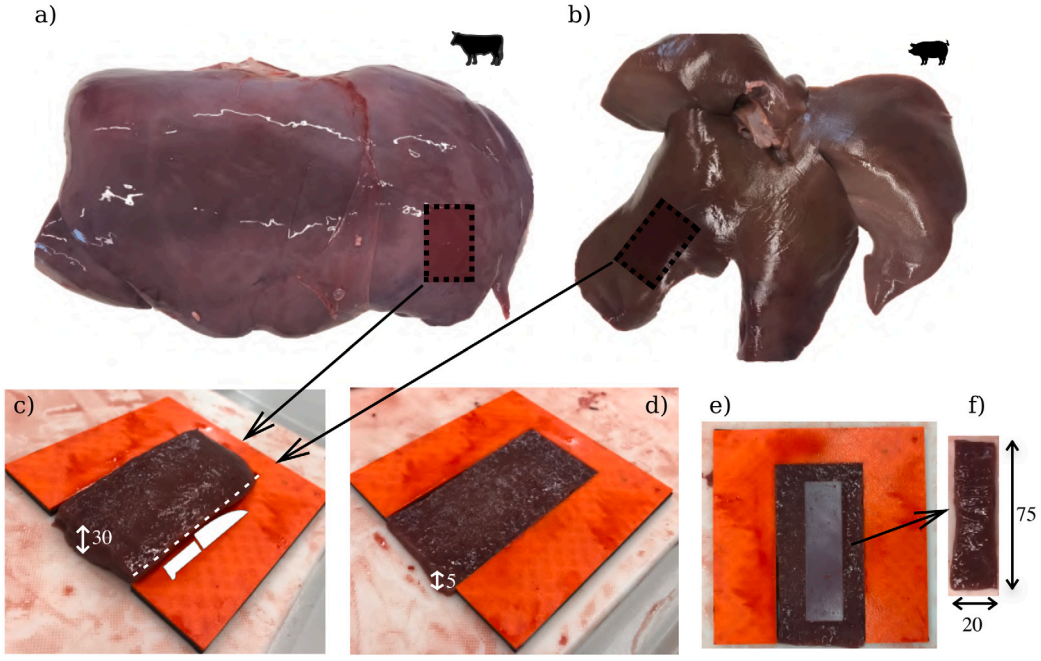

Fig. 1. Sample preparation: (a) and (b) whole bovine and porcine organs; (c) block of hepatic tissue is placed in the 3D printed cutting guide; (d) cutting along the surface of the cutting guide yields a thin tissue layer; (e) rectangular stencil is placed on the tissue layer; (f) sample that is cut from the tissue layer (75 × 20 × 5 mm).

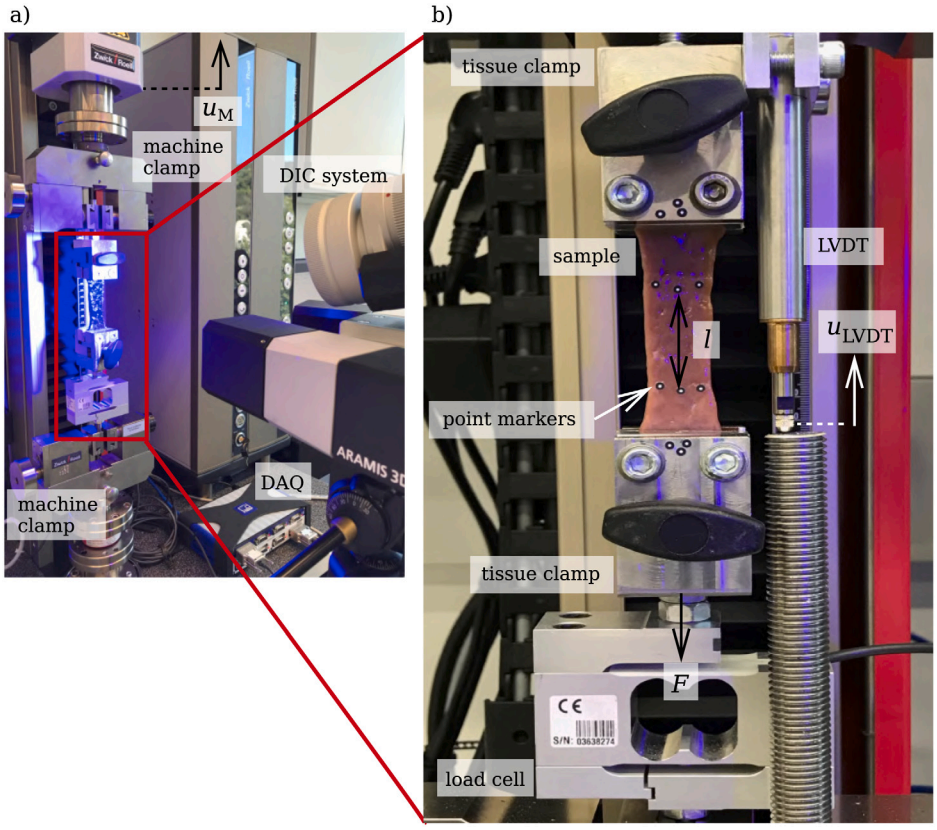

Fig. 2. Overview of the mechanical test setup: (a) the complete setup with the machine displacement u_M, upper and lower machine clamps, digital image correlation (DIC) system, and data acquisition module (DAQ) — connected to the load cell and displacement sensor (LVDT) in (b); furthermore in (b), hepatic sample clamped with the tissue clamps, point markers to measure the length l, the tensile force F, and the displacement of the LVDT u_{LVDT}.

For the evaluation of the dynamic cyclic tests, extremely small phase shifts between force and displacement of a few milliseconds need to be measured, requiring perfectly synchronous measurements. Thus, a linear variable differential transformer (LVDT) position sensor (Hottinger Baldwin Messtechnik GmbH, Darmstadt, Germany) was also connected to the same DAQ, for measuring displacement u_{LVDT} at exactly the same time as the load cell measurement.

The LVDT displacement, however, does not only describe tissue displacement, but also includes contributions stemming from machine and setup stiffness as well as clamping of the sample. For this reason, a specific measuring length l was defined with point markers on the sample whose change in length was recorded optically by the digital image correlation (DIC) system ARAMIS (GOM GmbH, Braunschweig, Germany). To certify uniform displacement within the sample, three marker pairs were arranged along the width of the sample and length l was reported as the average of the three distances. Actual tissue strains were based on these DIC displacements, while the temporal information, needed for the dynamic cyclic tests was extracted from the LVDT measurement.

An overview of the mechanical test setup and the measured properties (force F, machine displacement u_M, position sensor displacement u_{LVDT}, and sample measuring length l) are depicted in Fig. 2.

A mounting procedure of the samples in the testing machine, similar to the one described by Manoogian et al. (2009) and Kemper et al. (2010), was followed: First the top tissue clamp was removed from the testing machine and the sample was placed on the sand paper surface of the clamp and aligned. Used sand paper was always replaced by a new layer for each sample. Next, the sample was inserted in the testing machine, attached to the top clamp with its bottom end hanging freely. At this stage, each sample was allowed to hang under its own weight (~0.08 N) for approximately 3 min to ensure an equal small preloading of the tissue. Finally the bottom clamp was carefully closed, the sticky markers for DIC were applied, and sample cross-section was measured with an analogue calliper at three locations along the measuring length. The initial cross-section A_0 was taken as the average of these three measurements. The initial length l_0 was defined based on a single DIC image taken before starting mechanical loading.

Each sample was exposed to one of the following mechanical tests: ramp test, stress relaxation, or dynamic cyclic test (Fig. 3). All 36 samples of the porcine and bovine tissue were divided among the three testing methods, resulting in 12 samples per test and tissue type.

Ramp test. Upon starting extension of the samples, a trigger signal was sent from the testing machine to the DIC system, prompting both measurements to start. The cross-head of the testing machine was displaced by $u_M = 10$ mm (resulting in a maximum engineering tissue strain of $0.10 - 0.14$) at a speed of 5 mm/min (corresponding to a strain rate of $\sim 0.001\ s^{-1}$) and then moved back to its initial position at the same speed (see Fig. 3a). Due to the highly strain rate dependent behaviour of soft biological tissues, evaluation of elastic properties requires *quasistatic* strain rates (Fung, 1967; Miller and Chinzei, 1997). A similar strain rate was utilized as the rate reported for hepatic capsule in tension by Brunon et al. (2010) who considers $0.001\ s^{-1}$ to be quasistatic. Force F, from the 100 N load cell, and lengths l between the markers, from DIC for calculating strains, were both recorded at a measuring rate of 10 Hz.

Stress relaxation. A cross-head displacement of $u_M = 5$ mm (~0.06 tissue strain based on DIC measurement) was applied within ~0.4 s and held for 300 s (see Fig. 3b). Force F and lengths l between the markers were both recorded at a rate of 10 Hz by the 100 N load cell and DIC, respectively.

Dynamic cyclic test. After capturing a single image with the DIC system for defining the initial length between the markers l_0, a cross-head displacement of $u_M = 6$ mm (~0.08 tissue strain) was applied and then held for 250 s to allow best possible relaxation. Next, sinusoidal displacements of ±0.5 mm (±0.006 tissue strain) were applied at $f = 0.5$, $f = 1.0$, $f = 1.5$, and $f = 2.0$ Hz for 100 cycles at each frequency. Low frequencies were chosen to avoid inertia effects (Nicolle and Palierne, 2010; Chatelin et al., 2011) and to represent tactile palpation of the material (Estermann et al., 2020). Samples were allowed to relax at $u_M = 6$ mm for 250 s between each tested frequency to enable comparison of the frequency-dependent tissue response. See Fig. 3c for an overview of the testing procedure.

The chosen strain level ensured that samples were not compressed but stayed in tension throughout the test. Lengths between markers l were recorded by the DIC system (at 10 Hz for $f = 0.5$ Hz and at 20 Hz for the other frequencies). Pretests showed that phase shifts between stress and strain were expected to be ~15 ms for liver. Thus, in order to resolve such small phase shifts, measuring of force and displacement must be perfectly synchronized. For this reason, u_{LVDT} from the LVDT was utilized alongside F from the load cell, both being controlled by the same data acquisition module and software at a sampling frequency of 100 Hz. The LVDT position sensor yielded the actual occurrence time of the displacement without delay, while DIC provided the accurate displacement (and strain) amplitude.

2.3. Data analysis

Uniaxial tissue stretch λ (in direction of the main sample axis) is expressed as the ratio between deformed length l and the initial length l_0 as

$$\lambda = \frac{l}{l_0} = \varepsilon + 1\,, \tag{1}$$

with ε being engineering strain. Cauchy (true) stress σ_T – assuming incompressibility of hepatic tissue (Chui et al., 2004) – and engineering stress σ_E were calculated based on the measured tensile force F and initial cross-section A_0 as

$$\sigma_T = \frac{F}{A_0}\lambda \tag{2}$$

and

$$\sigma_E = \frac{F}{A_0}\,. \tag{3}$$

Ramp test. Hepatic parenchyma tissue is viscoelastic, exhibiting hysteresis even during extremely slow loading and unloading cycles. Thus, a purely hyperelastic treatment of the material is not valid, as this would completely ignore viscoelasticity. The so-called pseudoelastic approach – introduced by Fung (1993) – allows the separate evaluation of the loading and unloading branch with two distinct sets of characteristic hyperelastic parameters.

In order to establish a stress–strain relation, in terms of a hyperelastic model, the strain energy function Ψ is introduced. For an isotropic material, $\Psi = \Psi(I_1, I_2, I_3)$ depends on the strain invariants I_1, I_2, and I_3. The strain invariants are calculated based on the finite deformation applied to the material. In the following sections, liver tissue is modelled as incompressible ($\nu = 0.5$), as is often done for soft tissues (Fung, 1967; Miller and Chinzei, 1997; Gao et al., 2010; Roan and Vemaganti, 2011). The Poisson's ratio of $\nu = 0.434 \pm 0.16$ for hepatic parenchyma in tension reported by Chui et al. (2004), furthermore supports the assumption of incompressibility.

Thermodynamic, symmetry, and energy considerations enable the choice of $\Psi(I_1, I_2, I_3)$. Based on the comparison of different hyperelastic models presented in Appendix A, the strain energy function suggested by Veronda and Westmann (1970) for feline skin was utilized:

$$\Psi = c_1\left[e^{\beta(I_1-3)} - 1\right] + c_2(I_2 - 3) + g(I_3)\,, \tag{4}$$

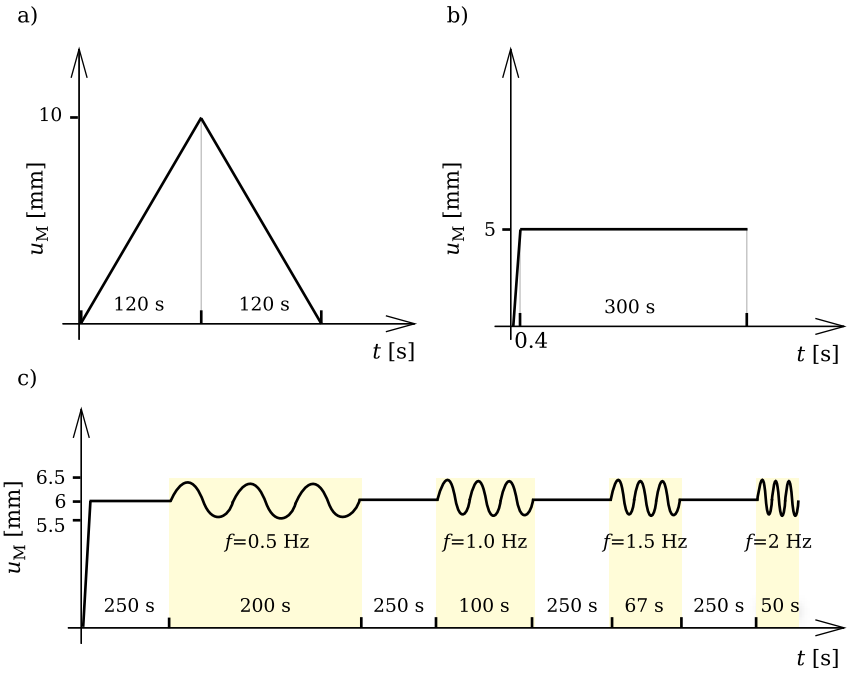

Fig. 3. Overview of the mechanical testing protocols with u_M being the machine displacement and t the time: (a) ramp loading and unloading sequence, (b) holding phase for relaxation, and (c) dynamic cyclic testing (100 cycles for each frequency).

with c_1, c_2, and β being the model parameters, and $g(I_3)$ being a function of tissue compressibility. After inserting the strain invariants $I_1 = \lambda^2 + \frac{2}{\lambda}$, $I_2 = 2\lambda + \frac{1}{\lambda^2}$, and $I_3 = 1$ for uniaxial tension of an incompressible material into Eq. (4) and further simplifying with $g(I_3) = g(1) = 0$, $c_2 = -c_1\frac{\beta}{2}$, and $c_1 = c$, the strain energy function results in

$$\Psi = c\left[e^{\beta(I_1-3)} - 1\right] - c\frac{\beta}{2}(I_2 - 3), \tag{5}$$

leaving the two material parameters c and β to be determined.

In case of incompressibility, the uniaxial Cauchy stress σ_T can be expressed in terms of the strain invariants I_1 and I_2, according to Holzapfel (2000), as

$$\sigma_T = 2\left(\lambda^2 - \frac{1}{\lambda}\right)\left(\frac{\partial\Psi}{\partial I_1} + \frac{1}{\lambda}\frac{\partial\Psi}{\partial I_2}\right), \tag{6}$$

Using Eqs. (5) and (6), the stress of the Veronda–Westmann model can thus be written as

$$\sigma_{VW} = 2\left(\lambda^2 - \frac{1}{\lambda}\right)c\beta\left(e^{\beta(I_1-3)} - \frac{1}{2\lambda}\right). \tag{7}$$

To now obtain material parameters for the loading and unloading part of the tensile ramp experiments, Eq. (7) was fit to the experimental true stress with non-linear least squares method, utilizing a Levenberg–Marquardt algorithm (Marquardt, 1963), for loading and unloading curves separately. Thus, the resulting fitting parameters were c_{load} and β_{load} (for loading) as well as c_{unload} and β_{unload} (for unloading). The coefficient of determination r^2 was calculated in order to evaluate how well the model data corresponded to the experimental data. See Fig. 4 for a typical experimental stress–stretch curve alongside the corresponding hyperelastic model.

In addition to the above described hyperelastic approach, a second type of data evaluation was applied, that is more descriptive of the stress–stretch curve shape. For each loading–unloading sequence, three characteristic elastic moduli were defined: E_I as the initial elasticity, E_{II} for the highest stretch during loading, and E_{III} for the first stretch during unloading. E_I, E_{II}, and E_{III} were calculated based on the slope of tangent of σ_{VW} for the corresponding stretch ranges (see Fig. 4).

Furthermore, the ramp tests were interpreted based on energy considerations: For stretching the material, mechanical work is required in the loading phase, which is partly dissipated and partly stored as elastic strain energy. During the following unloading phase, part of the stored energy is recovered elastically while another part is dissipated. The ratio between the dissipated energy density W_{dis} and the recovered (or stored) energy density W_{st} is referred to as *relative dissipation*, W_{dis}/W_{st}, and can be calculated based on the stress–stretch curves. Thereby, W_{dis} is the area between the loading and unloading curve and W_{st} is the area under the unloading curve (see Fig. 4). Due to energy considerations, however, engineering stress σ_E with the stretch ratio λ as its energy conjugate (Shergold et al., 2006) were used for these calculations (Fig. 4).

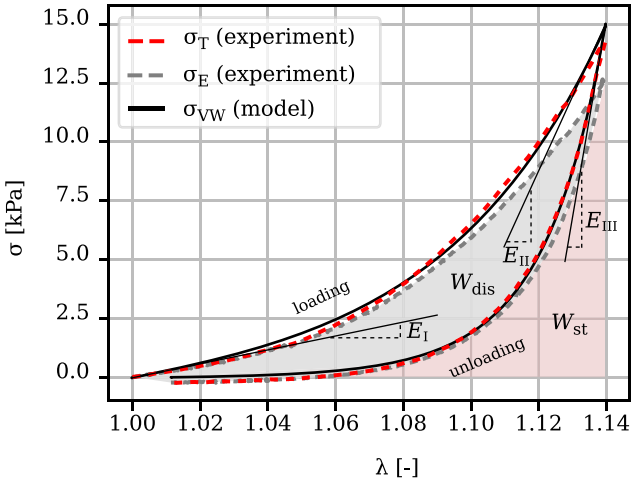

Fig. 4. Typical stress–stretch curve of a bovine ramp test with the measured true stress σ_T (dashed red line), the corresponding Veronda-Westmann curve fit σ_{VW} (solid black line), and the calculated elastic moduli (E_I, E_{II}, and E_{III}). The engineering stress σ_E (dashed grey line) is used to calculate the dissipated energy density W_{dis} and stored energy density W_{st}.

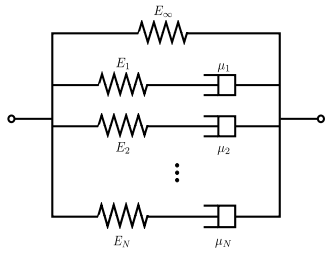

Fig. 5. Generalized Maxwell model, consisting of the longterm elastic modulus E_∞ and the N parallel Maxwell branches with springs E_1, E_2, ... E_N and dashpots μ_1, μ_2, ... μ_N.

Stress relaxation. Assuming a step displacement, where the holding phase is reached instantaneously, stress σ and the constant strain ε_0 are connected via the time-dependent relaxation function $E(t)$ according to

$$\sigma(t) = E(t)\varepsilon_0 \,. \tag{8}$$

The relaxation function can be approximated in terms of Prony series,

$$E(t) = E_\infty + \sum_{i=1}^{N} E_i e^{-\frac{t}{\tau_i}} \,, \tag{9}$$

which correspond to the generalized Maxwell model depicted in Fig. 5, with the longterm elastic modulus E_∞, the elastic moduli of the springs E_i, and the characteristic relaxation times τ_i (which are related to the dashpot viscosities μ_i via $\tau_i = \mu_i/E_i$) (Findley et al., 1989). Replacing E_∞ by

$$E_\infty = E_0 - \sum_{i=1}^{N} E_i \,, \tag{10}$$

in Eq. (9), expresses the relaxation function in terms of the initial elasticity E_0 (the ratio between stress and strain at the beginning of the holding phase) according to

$$E(t) = E_0 - \sum_{i=1}^{N} E_i(1 - e^{-\frac{t}{\tau_i}}) \,. \tag{11}$$

After inserting Eq. (11), Eq. (8) was utilized to approximate the experimental stress relaxation, applying a non-linear least squares method, implemented with a trust region reflective algorithm, which limited fitting parameters to positive values. Thereby, the curve fit was performed over the complete holding time of 300 s, as discussed below and in Appendix B. Furthermore, based on considerations presented in Appendix B, $N = 3$ was chosen for further calculations, as was also done by Ocal et al. (2010) for compression and Estermann et al. (2020) for indentation of hepatic tissue in the context of relaxation within the same magnitude of holding times.

Obtained, model parameters E_i and τ_i were then utilized to calculated the storage and loss moduli E' and E'' according to Gutierrez-Lemini (2014) with

$$E' = E_\infty + \sum_{i=1}^{N} \frac{E_i \omega^2 \tau_i^2}{1 + \omega^2 \tau_i^2} \tag{12}$$

and

$$E'' = \sum_{i=1}^{N} \frac{E_i \omega \tau_i}{1 + \omega^2 \tau_i^2} \,, \tag{13}$$

where ω is the angular frequency. The ratio of loss modulus to storage modulus

$$\frac{E''}{E'} = \tan\delta = \sum_{i=1}^{N} \frac{\omega \mu_i E_i^2}{E_\infty(E_i^2 + \omega^2 \mu_i^2) + \omega^2 E_i \mu_i^2} \tag{14}$$

is called *loss tangent* $\tan\delta$, which is a characteristic viscoelastic property that describes the frequency-dependent material damping behaviour.

Concerning the Prony series curve fit the question arises whether holding duration influences the resulting viscoelastic properties. The reason for this being the following: Data was sampled equidistantly throughout the holding phase of 300 s. Thus, the portion of rapid stress decline at the beginning of the stress-time curve is emphasized less in the curve fit, in contrast to the portion of nearly constant stress in the middle and end part of the curve, where many more data points are available. Further examination of the influence of holding time is described in Appendix B, showing that $\tan\delta$ is fairly consistent throughout the tested time span. Thus, if not further specified, $\tan\delta$ is reported for a holding time of 300 s in the following sections.

Additionally to the frequency-dependent damping behaviour expressed by $\tan\delta$ and the dynamic moduli E' and E'', relative dissipation $\frac{W_{\text{dis}}}{W_{\text{st}}}$ is calculated for the performed experiment. The work density, necessary for initially reaching ε_0 during the fast ramp loading, can be expressed as

$$W_0 = \frac{1}{2} E_0 \varepsilon_0^2 \,, \tag{15}$$

with $E_0 = E_\infty + E_1 + E_2 + E_3$ (Eq. (10)) referring to the parallel springs in Fig. 5. After waiting for the holding period to pass and the viscosities to dissipate, the only spring contributing to the stress response is the long-term stiffness E_∞, meaning that the work, which can be elastically recovered if the material were unloaded at this point, is

$$W_{\text{st}} = \frac{1}{2} E_\infty \varepsilon_0^2 \,. \tag{16}$$

Thus, the dissipated energy density, being the difference between W_0 and W_∞, can be expressed as

$$W_{\text{dis}} = \frac{1}{2}(E_1 + E_2 + E_3)\varepsilon_0^2 \,. \tag{17}$$

Finally, the relative dissipation $W_{\text{dis}}/W_{\text{st}}$ results in

$$\frac{W_{\text{dis}}}{W_{\text{st}}} = \frac{E_1 + E_2 + E_3}{E_\infty} \,. \tag{18}$$

Dynamic cyclic test. The analysis of dynamic cyclic tests consists of finding $\tan\delta$, E', and E'' from sinusoidal data. For a linear viscoelastic material exposed to a sinusoidal displacement

$$u(t) = u_{\text{A}} \sin(\omega t) \tag{19}$$

with the displacement amplitude u_{A}, angular frequency ω, and time t, the responding force is also sinusoidal with the same frequency and amplitude F_{A} but shifted by a phase δ (Fig. 6a)

$$F(t) = F_{\text{A}} \sin(\omega t + \delta) \,. \tag{20}$$

Due to the fact that phase shifts are expected to be in the range of a few milliseconds, special attention needs to be taken concerning the synchronicity of the force and displacement measurement. Thus, the loss tangent $\tan\delta$ was based on LVDT displacements. Non-linear least squares method was utilized to fit Eqs. (19) and (20) to F and u_{LVDT}, yielding the fitting parameters F_{A}, u_{A}, ω, and δ. This method was applied to the last 30 cycles of each frequency test, leaving the first 70 cycles for preconditioning the material to a steady state oscillation.

Furthermore, after utilizing u_{LVDT} for calculating $\tan\delta$, storage and loss modulus E' and E'' were calculated using strains ε based on the DIC measurement with

$$E' = \frac{\sigma_{\text{A}}}{\varepsilon_{\text{A}}} \cos\delta \tag{21}$$

and

$$E'' = \frac{\sigma_{\text{A}}}{\varepsilon_{\text{A}}} \sin\delta \,, \tag{22}$$

with ε_{A} being the amplitude of engineering strain and σ_{A} being the amplitude of true stress. Description of the measured quantities can be found in Fig. 6b.

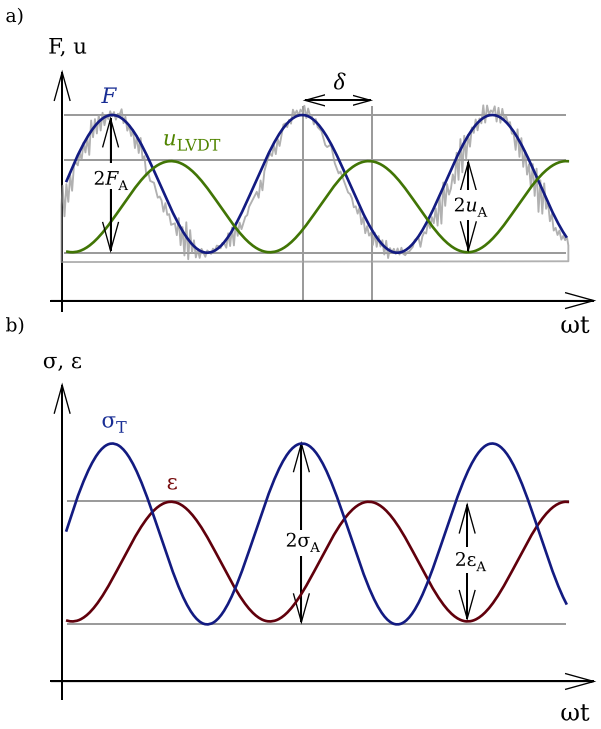

Fig. 6. Schematic overview of the analysis of the dynamic tests: (a) the LVDT displacement and the load cell force are utilized to identify the phase shift δ due to their perfect measuring synchronicity; (b) accurate signal amplitudes, ε_A and σ_A, are extracted from the strain, based on the DIC measurement, and the true stress, based on the load cell force.

In order to describe the loss factor in terms of energy dissipation, $\tan\delta$ can be written as the ratio between dissipated energy density and maximum stored energy density (Roylance, 2001):

$$2\pi \tan\delta = \frac{W_{dis}}{W_{st}}. \tag{23}$$

Thus, the relative dissipation W_{dis}/W_{st} per cycle is calculated, base on the obtained $\tan\delta$. In case of linear viscoelasticity, it is assumed that the energy dissipation stems from viscous effects only and not plastic behaviour.

2.4. Statistical analysis

Mean values and standard deviations were calculated over 12 bovine and 12 porcine samples for every result:

- from ramp tests the pseudoelastic parameters (c_{load}, β_{load}, c_{unload}, β_{unload}), elastic moduli (E_I, E_{II}, E_{III}), and W_{dis}/W_{st}
- from relaxation the Prony parameters (E_0, E_i, τ_i for $i = 1, 2, 3$), viscoelastic properties (E', E'', $\tan\delta$), and W_{dis}/W_{st}
- and from DMA at 4 frequencies the viscoelastic properties (E', E'', $\tan\delta$), and W_{dis}/W_{st}.

For comparing the two methods of viscoelastic characterization, the resulting viscoelastic properties $\tan\delta$, E', and E'' of relaxation and DMA were checked for normal distribution (Shapiro–Wilk test). Then, given normality, Welch's t-tests were performed to identify significant differences ($\alpha = 0.05$) between the measured properties for $\tan\delta$, E', and E'' at $f = 0.5$, $f = 1.0$, $f = 1.5$, and $f = 2.0$ Hz, depending on the experimental modality without the requirement of homogeneous variances.

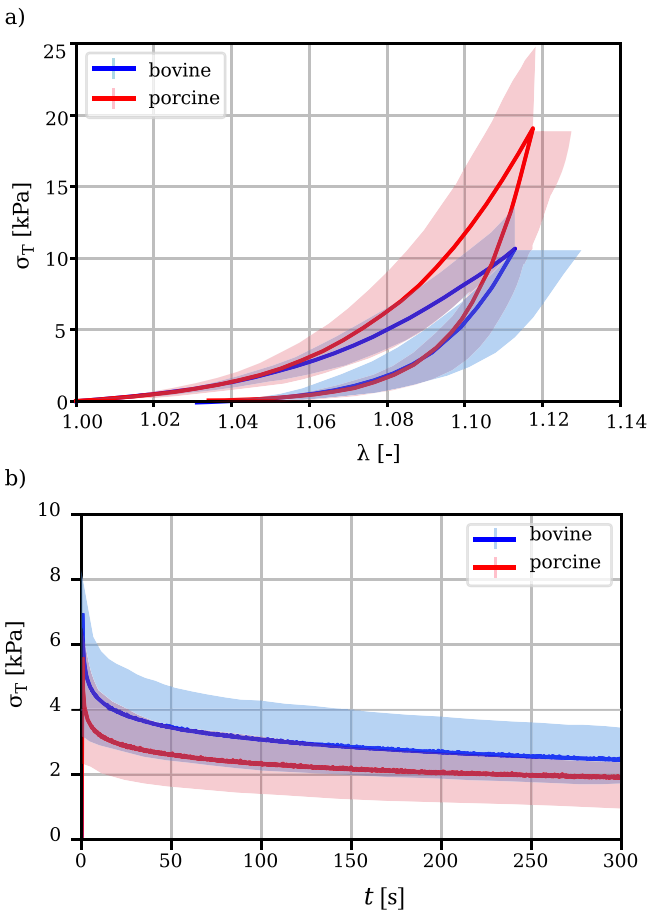

Fig. 7. (a) Mean true stress σ_T plotted over the mean stretch λ for the ramp tests with the shaded areas being the standard deviations of stress and stretch ($n = 12$ for bovine and $n = 12$ for porcine) and (b) the mean true stress σ_T plotted over time t for the relaxation tests, with the shaded area being the standard deviation of stress ($n = 12$ for bovine and $n = 12$ for porcine).

3. Results

Ramp test. The average values and standard deviations of true stress and stretch resulting from the loading–unloading sequence were plotted for all samples of the two tissue types in Fig. 7a. The characteristic mean stress–stretch curves of porcine and bovine tissue are visibly different from each other with the average maximum stress for porcine tissue being 19.15 kPa and for bovine tissue 10.69 kPa. The maximum average strain applied to the samples was ~11 %.

The experimental curves – exhibiting non-linearity and hysteresis – were interpreted with a pseudoelastic Veronda–Westmann model with the resulting parameters for the loading and unloading part given in Table 1. The coefficient of determination being around 0.998 for bovine as well as porcine tissue, signifies an excellent agreement between experimental data and model. Parameters c_{load} and c_{unload} can be interpreted as shear-like moduli with β_{load} and β_{unload} being dimensionless exponential parameters (Limbert, 2019). The initial zero-strain shear-like modulus c_{load} was higher for bovine tissue (0.542 ± 0.190 kPa) than for porcine tissue (0.353 ± 0.237 kPa).

Based on the pseudoelastic model, elastic moduli at different strain values were calculated (Table 1). While, the initial stiffness E_I was nearly the same for porcine and bovine tissue, the average elastic moduli for larger strains E_{II} and unloading E_{III} were more than twice as high for porcine liver. For the ramp loading and unloading sequence, the ratio between dissipated and stored energy density was calculated and results are given in Table 1. The relative energy dissipation being

Table 1
Results of the ramp tests for bovine and porcine tissue, given as mean values and standard deviations: parameters of the pseudoelastic Veronda-Westmann model c_{load}, β_{load}, c_{unload}, and β_{unload}, the coefficient of determination r^2, elastic moduli E_I, E_{II}, and E_{III}, and relative dissipation W_{dis}/W_{st}.

Tissue	c_{load} [kPa]	β_{load} [–]	c_{unload} [kPa]	β_{unload} [–]	r^2 [–]	E_I [kPa]	E_{II} [kPa]	E_{III} [kPa]	W_{dis}/W_{st} [–]
Bovine	0.542 ± 0.190	21.76 ± 8.953	0.013 ± 0.007	85.13 ± 23.97	0.998	32.00 ± 11.18	283.9 ± 92.94	689.6 ± 221.5	1.129 ± 0.177
Porcine	0.353 ± 0.237	35.11 ± 15.39	0.009 ± 0.008	101.50 ± 26.54	0.998	29.77 ± 14.79	669.9 ± 299.7	1428.4 ± 512.9	1.052 ± 0.285

Table 2
Results of the stress relaxation tests for bovine and porcine tissue, given as mean values and standard deviations: parameters of the Prony series fit ($N = 3$) E_0, E_1, τ_1, E_2, τ_2, E_3, and τ_3, the resulting root-mean-square error RMSE, and the relative dissipation W_{dis}/W_{st}.

Tissue	E_0 [kPa]	E_1 [kPa]	τ_1 [s]	E_2 [kPa]	τ_2 [s]	E_3 [kPa]	τ_3 [s]	RMSE [kPa]	W_{dis}/W_{st} [–]
Bovine	117.96 ± 30.24	33.92 ± 8.85	0.58 ± 0.15	20.16 ± 5.67	11.07 ± 0.83	26.61 ± 6.81	140.48 ± 6.84	0.03 ± 0.01	2.17 ± 0.14
Porcine	129.89 ± 64.91	44.19 ± 20.34	0.34 ± 0.19	22.08 ± 12.04	7.33 ± 2.04	24.98 ± 13.83	115.80 ± 22.29	0.04 ± 0.01	2.64 ± 0.71

Table 3
Relative dissipation W_{dis}/W_{st}, loss tangent $\tan\delta$, storage modulus E', and loss modulus E'' for the tested frequencies of bovine and porcine tissue.

		$f = 0.5$ Hz	$f = 1.0$ Hz	$f = 1.5$ Hz	$f = 2.0$ Hz
Bovine	W_{dis}/W_{st} [–]	0.603 ± 0.183	0.683 ± 0.335	n.a.	n.a.
	$\tan\delta$ [–]	0.096 ± 0.029	0.121 ± 0.067	n.a.	n.a.
	E' [kPa]	172.9 ± 88.74	158.4 ± 83.34	n.a.	n.a.
	E'' [kPa]	17.08 ± 9.975	17.55 ± 9.565	n.a.	n.a.
Porcine	W_{dis}/W_{st} [–]	0.611 ± 0.086	0.662 ± 0.283	0.696 ± 0.241	0.675 ± 0.254
	$\tan\delta$ [–]	0.097 ± 0.012	0.114 ± 0.061	0.117 ± 0.017	0.102 ± 0.046
	E' [kPa]	527.2 ± 172.2	488.3 ± 163.9	556.3 ± 205.6	509.8 ± 163.5
	E'' [kPa]	50.76 ± 16.75	52.23 ± 28.91	64.59 ± 25.49	48.00 ± 20.31

around $W_{dis}/W_{st} \sim 1.1$ for both tissue types, signifies that a similar amount of energy was dissipated due to viscosity and plasticity as stored elastically.

Stress relaxation. Characteristic stress relaxation curves were plotted in Fig. 7b for bovine and porcine tissue by averaging the true stress of all tested samples for each time instance. Prony series were fit to these experimental curves, yielding the model parameters given in Table 2. The resulting relaxation times represent 3 orders of magnitude with average $\tau_1 = 0.58$ s, $\tau_2 = 11.07$ s, and $\tau_3 = 140.48$ s for bovine tissue and average $\tau_1 = 0.34$ s, $\tau_2 = 7.33$ s, and $\tau_3 = 115.80$ s for porcine tissue. Relaxation times were shorter for porcine tissue compared to bovine tissue for each time scale.

Relative dissipation for bovine and porcine tissue was $W_{dis}/W_{st} > 2$ (Table 2), meaning that more than twice as much energy was dissipated during relaxation than stored elastically in the material. Porcine hepatic tissue exhibited W_{dis}/W_{st} around 20% higher than bovine tissue which is also mirrored in the trend that porcine $\tan\delta$ is higher than bovine $\tan\delta$ (Fig. 8). Thus, the relaxation results indicate that porcine hepatic tissue exhibits a higher viscous contribution than bovine tissue.

Dynamic cyclic test. For identifying the phase shift δ between force and displacement, sine curves were fit to the experimental force data F and the displacement of the position sensor u_{LVDT}. Due to the noisiness of the force readings for the two higher frequencies and due to the fact that the force level of bovine samples was even lower than porcine samples, the analysis for bovine tissue at $f = 1.5$ Hz and $f = 2.0$ Hz was not possible in the current setup. Dynamic viscoelastic properties are thus given for $f = 0.5$, $f = 1.0$, $f = 1.5$, and $f = 2.0$ Hz for porcine tissue and for $f = 0.5$ and $f = 1.0$ Hz for bovine tissue in the following sections. Due to the pre-stress and the small oscillatory amplitudes, samples were under tension throughout the whole experiment.

Table 3 lists the relative dissipation W_{dis}/W_{st} depending on the tested frequency for both tissue types, showing that on average $W_{dis}/W_{st} = 0.64$ for bovine and $W_{dis}/W_{st} = 0.66$ for porcine liver. $W_{dis}/W_{st} < 1$ means that more energy was recovered elastically than dissipated due to viscosity for each cycle.

Furthermore, given in Table 3, are the mean values and standard deviations of the viscoelastic properties $\tan\delta$, E', and E'' found for bovine and porcine hepatic tissue in the dynamic tests.

Comparison of the viscoelastic parameters. Loss tangent, storage modulus and loss modulus were extracted from relaxation, as well as DMA tests. Figs. 8–10 depict the frequency dependence of $\tan\delta$, E', and E'' as was calculated based on the generalized Maxwell model for relaxation and measured in DMA. Porcine and bovine loss tangents correspond very well for the different testing methods throughout the examined frequency range (Figs. 8a and b). When regarding the porcine storage modulus (Fig. 9a), however, a discrepancy between relaxation ($E' \sim 100$ kPa) and dynamic cyclic testing ($E' \sim 500$ kPa) becomes apparent for all tested frequencies. Bovine tissue, on the other hand, yielded storage moduli that matched well for the testing methods (Fig. 9b). A similar trend can be observed, concerning E'': While for porcine tissue, the dynamic loss modulus was more than two times higher than that found in relaxation (Fig. 10a), bovine tissue exhibited E'' relatively independent of the testing method (Fig. 10b).

Regarding a given frequency, for instance 1 Hz, the loss tangent $\tan\delta$ was not significantly different depending on the type of test for porcine ($p = 0.3$) or bovine tissue ($p = 0.07$). The viscoelastic moduli E' and E'' found in dynamic tests, however, were significantly higher than the relaxation E' and E'' for porcine tissue at 1 Hz ($p = 0.000006$ and $p = 0.002$). For bovine tissue at 1 Hz, only E'' was significantly different depending the testing method ($p = 0.01$), while E' was statistically the same for relaxation and cyclic testing ($p = 0.1$).

4. Discussion

For evaluating liver mechanical properties, different tests were performed in tension on bovine and porcine hepatic parenchyma samples. In order to describe non-linear as well as viscoelastic behaviour, mechanical testing consisted of ramp loading and unloading, stress relaxation, and DMA. In the following section, the resulting properties from the different tests are discussed and finally the two viscoelastic testing methods (stress relaxation and DMA) are compared with each other.

Ramp test. The ramp stress–stretch curves were interpreted based on a hyperelastic modelling approach, utilizing a Veronda-Westmann strain energy function.

Chui et al. (2004) examined different strain energy functions for hyperelastic modelling of combined compression and elongation of porcine liver parenchyma at a much faster strain rate of ~0.03 s^{-1} than the current study (~0.001 s^{-1}), however without modelling unloading. The Veronda-Westmann model thereby yielded average parameters of $c = 0.07$ kPa and $\beta = 4.5$, which are lower than the current results ($c_{load} \sim 0.35$ kPa and $\beta_{load} \sim 35.1$ for porcine tissue). The differing model parameters could be attributed to the higher strain rate, used by Chui et al. (2004). Interestingly, it is counterintuitive that the stiffness would be lower for higher strain rates. The results furthermore differ when comparing the magnitude of stress found for similar strains, with Chui et al. (2004) obtaining much smaller stresses than stresses measured in the current study. Other publications (Lu et al., 2014; Dunford et al., 2018) reported similar stress magnitudes as found in the

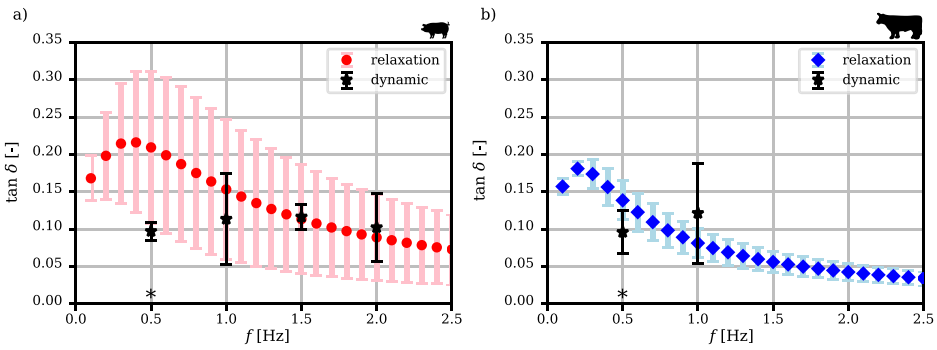

Fig. 8. Loss tangent $\tan\delta$ and standard deviation measured in dynamic cyclic tests for different frequencies plotted alongside $\tan\delta$, based on relaxation data, calculated for different frequencies with the generalized Maxwell model for (a) porcine hepatic tissue ($n = 12$ for relaxation and $n = 12$ for dynamic) and (b) bovine tissue ($n = 12$ for relaxation and $n = 12$ for dynamic), asterisks marking frequencies at which the properties found in the two testing methods were significantly different ($\alpha = 0.05$).

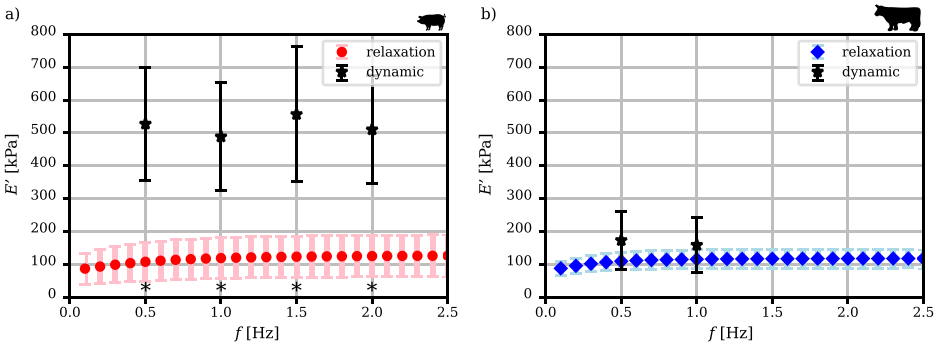

Fig. 9. Storage modulus E' and standard deviation measured in dynamic cyclic tests for different frequencies plotted alongside E', based on relaxation data, calculated for different frequencies with the generalized Maxwell model for (a) porcine hepatic tissue ($n = 12$ for relaxation and $n = 12$ for dynamic) and (b) bovine tissue ($n = 12$ for relaxation and $n = 12$ for dynamic), asterisks marking frequencies at which the properties found in the two testing methods were significantly different ($\alpha = 0.05$).

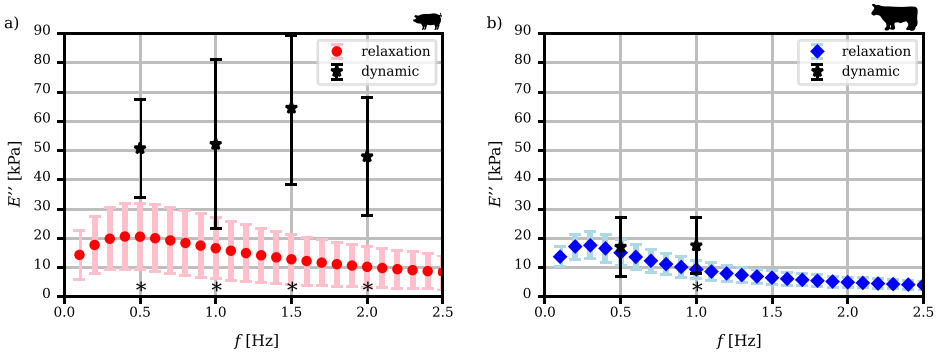

Fig. 10. Loss modulus E'' and standard deviation measured in dynamic cyclic tests for different frequencies plotted alongside E'', based on relaxation data, calculated for different frequencies with the generalized Maxwell model for (a) porcine hepatic tissue ($n = 12$ for relaxation and $n = 12$ for dynamic) and (b) bovine tissue ($n = 12$ for relaxation and $n = 12$ for dynamic), with asterisks marking frequencies at which the properties found in the two testing methods were significantly different ($\alpha = 0.05$).

current study, even though strain rates were also higher with $0.01\,s^{-1}$. This discrepancy between stress response found in Chui et al. (2004) and other publications could be explained by differences in sample fixation strategies during testing: For example, Chui et al. (2004) glued the samples to movable plates while Lu et al. (2014), Dunford et al. (2018), and the here-presented study utilized tissue clamps. Another difference is that Chui et al. (2004) reported stretch based on the machine displacement, while the other mentioned studies utilized optical measurement.

The current loading curves of the ramp tests were nearly linear for small strains up to ~3% (see Fig. 7a), which is similar to behaviour reported by Hollenstein et al. (2006) and Snedeker et al. (2005), who calculated initial stiffness up to 2% and 5% for hepatic and renal capsule tissue, which means that a single modulus E_I can describe tensile behaviour of liver up to a strain of 3% with sufficient accuracy. Furthermore, it can be observed that the parenchyma is much softer than the capsule when comparing $E_I \sim 30$ kPa for bovine and porcine tissue, found in the current study, with the values reported for capsule of ~1100 kPa (Hollenstein et al., 2006). This huge difference shows that for complete liver characterization, capsule as well as parenchyma need be examined.

While E_I was the same for porcine and bovine tissue, stiffness differences between the two tissues only became apparent for higher strains in E_{II} and E_{III}. This could be due to histological differences of the tissues: Porcine hepatic tissue exhibits a higher content of collagen than bovine tissue (Neuman and Logan, 1950), which is the main structural protein in healthy liver due to elastin content being very low (Kanta, 2016). While elastin mainly contributes to the initial stiffness in the initial linear region of the stress–stretch curve, collagen characterizes the tissue stiffness for higher strains (Duong et al., 2015). Thus, the

higher stiffness in E_{II} and E_{III} of porcine liver could be explained by its higher collagen content compared to bovine liver.

Regarding the comparison of animal and human hepatic tissue, Kemper et al. (2010) tested human liver parenchyma in uniaxial tension at different strain rates, showing that failure stress and stretch were very similar to bovine but significantly different to porcine hepatic tissue by comparing their results with Santago et al. (2009) for bovine and with Uehara (1995) for porcine tissue. Thus, it would be interesting to further investigate the similarity between the tissue types, not only for failure properties but also for stiffness in sub-failure strain ranges. Concerning its collagen distribution, human liver corresponds better to bovine than porcine liver (Zhang, 1999; Eurell and Frappier, 2006; Lowe and Anderson, 2015), which might lead to similar stiffness of human and bovine tissue, especially in terms of E_{II} and E_{III}. This, however, still remains to be shown in future research.

The resulting relative dissipation of around 1 for porcine and bovine tissue indicated that liver tissue is highly viscoelastic, which motivated the detailed analysis via relaxation and dynamic cyclic testing.

Stress relaxation. In order to quantify the viscous properties of liver tissue that already became visible as hysteresis and, with that, energy dissipation in the ramp tests, stress relaxation experiments were performed.

The stress decline over time was modelled with a 3-element Prony series and viscoelastic properties $\tan\delta$, E', and E'' were calculated in the frequency domain. Resulting mean $\tan\delta = 0.07 - 0.22$ for porcine and mean $\tan\delta = 0.05 - 0.17$ for bovine tissue corresponded very well to previously published values. For instance, the loss tangent has previously been reported to be in a range of $0.20 - 0.25$ for dynamic compression of canine liver (Kiss et al., 2004), dynamic shear of porcine and murine liver (Wex et al., 2014; Zhang et al., 2017), and indentation relaxation of porcine and bovine liver (Estermann et al., 2020).

Average storage and loss moduli for porcine as well as bovine hepatic tissue of around $E' \sim 100$ kPa and $E'' = 5 - 20$ kPa found in the current study match the values reported by Ocal et al. (2010) for bovine liver in compression ($E' \sim 75$ kPa and $E'' \sim 10$ kPa after 48 h preservation for comparable frequencies) well.

Furthermore, the absolute value of the complex modulus $|E^*| = \sqrt{E'^2 + E''^2} = 10 - 40$ kPa was reported by Zhang et al. (2007) for compression tests on bovine liver, which is lower than the $|E^*| \sim 100$ kPa of the current study. However, Zhang et al. (2007) refrigerated the cut samples over night in saline solution before testing, which could have lead to a decrease in stiffness (Dunford et al., 2018).

Kiss et al. (2004) reported $E' = 50$ kPa and $E'' = 10$ kPa for $f = 1.0$ Hz in dynamic compression of canine liver, with E' being lower than the current values and E'' matching very well. The lower stiffness concerning the storage modulus could be associated with differences between the hepatic tissue types or differences between compression and tension.

For all conducted experiments, the relative dissipation was calculated, yielding the highest values of W_{dis}/W_{st} for relaxation, compared to ramp testing and DMA. W_{dis}/W_{st} describes tissue behaviour in a specific experimental framework and is not understood as material property. Differences in relative dissipation are caused by inherent differences in the loading methods and cannot be compared directly between the methods. For instance, relative dissipation of stress relaxation is not frequency-dependent and describes viscoelasticity in a temporal sense. Relative dissipation of DMA, on the other hand, was calculated depending on the frequency. However, W_{dis}/W_{st} can be used as a straightforward parameter for comparing materials that were tested with the same method.

Dynamic cyclic testing. Additionally to stress relaxation, DMA was conducted as the gold standard in terms of measuring viscoelastic properties. The large strain ramp tests yielded notable hyperelastic behaviour in their stress–stretch plots. However, due to the fact that the strain amplitudes used for DMA were very small (0.6%), linear elastic behaviour was assumed for the given prestrain level (8%) for the DMA tests in the range of the amplitude.

The sinusoidal stress and strain curves directly yielded the viscoelastic properties $\tan\delta$, E', and E'' for different frequencies ($f = 0.5$, $f = 1.0$, $f = 1.5$, and $f = 2.0$ Hz for porcine tissue and $f = 0.5$ and $f = 1.0$ Hz for bovine tissue). No clear trend, concerning the influence of frequency on the measured properties, could be observed (Figs. 8–10). A much larger range of frequencies is necessary to accurately evaluate the frequency-dependent behaviour, for example using a shear rheometer (Zhu et al., 2013; Wex et al., 2014; Zhang et al., 2017). Nevertheless, the here-presented method proved feasible for probing a few distinct frequencies of interest.

The tensile dynamic loss tangent of the current study matches $\tan\delta$ for compression, shear, and indentation found in literature (Kiss et al., 2004; Wex et al., 2014; Zhang et al., 2017; Estermann et al., 2020). However, no other studies conducted in tension were found, for comparing the current results of tensile storage E' and loss moduli E'' directly.

As discussed above, storage and loss moduli from compressive experiments corresponded to the current results for E' and E'' agreeably well for stress relaxation of bovine tissue. Furthermore, bovine tissue yielded similar results in DMA as in stress relaxation. However, results based on DMA for porcine tissue were higher than previously published results for E' and E'' in compression (Kiss et al., 2004; Zhang et al., 2007; Ocal et al., 2010). This discrepancy could mean that there is a larger difference between tensile and compressive properties for porcine tissue than bovine liver.

Experiments, concerning viscoelasticity of human liver, by Lim et al. (2009) yielded $\tan\delta \sim 0.6$ for 1 Hz. However, these results were obtained via dynamic indentation on the whole intact organ, including contributions from the capsule and under different boundary conditions. Thus, to compare $\tan\delta$, E', and E'' of human hepatic tissue to the current results, human liver needs to be tested with the same or similar method.

Concerning relative dissipation, W_{dis}/W_{st} was calculated for each tested frequency. When comparing W_{dis}/W_{st} between porcine and bovine tissue, no significant difference can be observed between the tissue types. Thus, based on the here-presented dynamic results alone, it cannot be concluded which tissue type is more viscous.

Comparison of the viscoelastic parameters. Hysteresis found in the ramp stress–stretch curves, motivated further examination of liver viscoelastic behaviour. Thus, stress relaxation and DMA were conducted for extracting storage and loss moduli, as well as loss tangent. While DMA is the gold standard, concerning the evaluation of these viscoelastic properties, it is connected to experimental difficulties. The following section should answer the question whether relaxation experiments can yield comparable results to DMA.

Stress relaxation experiments, consisting of a single holding phase, were easier to conduct compared to the dynamic tests: For example, in DMA the temporal stress and strain resolution was of essence as phase shifts of ~15 ms had to be measured, thus demanding an additional LVDT position sensor. The DIC system which yields the accurate magnitude of strains does not necessarily coincide perfectly in a temporal sense with the displacement of the machine.

Usually, DMA is conducted on rheometers designed specifically for this type of experiment. However, the current setup consisted of a universal testing machine. Even though only limited testing frequencies and no temperature variations were possible, we were able to conduct the experiments without using a rheometer.

Ocal et al. (2010) also calculated storage and loss moduli based on relaxation data as well as on dynamic cyclic testing for bovine hepatic tissue, finding a good agreement between the two testing methods. However their experiments were conducted in compression.

Concerning both porcine and bovine tissue, $\tan\delta$ was statistically indiscernible depending on the testing method in the current study

(Fig. 8). Big differences in testing method, however, became visible for porcine liver when regarding E' and E'' (Figs. 9a and 10a), while agreement for E' and E'' of bovine tissue was good (Figs. 9b and 10b). Stress relaxation was conducted at 6% tissue strain while dynamic cyclic testing was done at a strain level of 8%. This difference in strain seems to be irrelevant for bovine tissue, which can be explained by the fairly linear behaviour in terms of elasticity in Fig. 7a; not however for porcine tissue which exhibits a more pronounced non-linear stress relation for 6–8% strain. This means that the difference between testing methods in porcine storage and loss moduli could be explained by the non-linear elastic behaviour found in the tested strain range, while loss tangent $\tan\delta$ was unaffected by the difference in strain level.

In conclusion, the comparison of stress relaxation and DMA results is feasible as long as elasticity non-linearities are kept in mind. The results showed that $\tan\delta$ is quite robust in terms of slight variations of strain level between relaxation and DMA, while E' and E'' are more severely affected. The here presented viscoelastic investigation is novel in its application to hepatic parenchyma and provides a guideline for evaluation of soft tissues mechanical properties in tension.

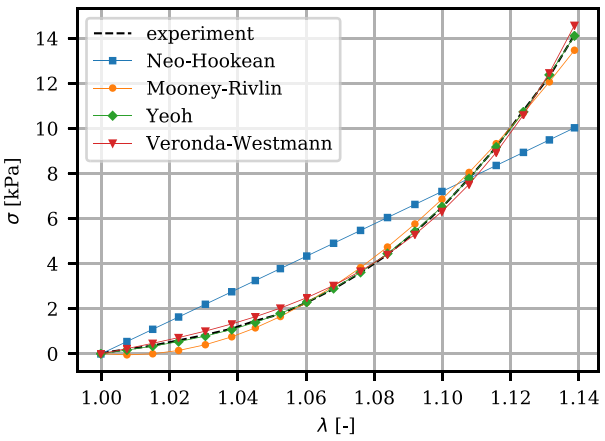

Fig. A.11. True stress–stretch curve of one bovine loading sequence fitted with different hyperelastic models.

5. Limitations

Following limitations of this study should be pointed out:

- Concerning the stress relaxation experiments, a perfect step displacement was assumed where the tissue is stretched instantaneously. A more sophisticated modelling approach, as suggested for example by Oyen (2005), would include the influence of the finite ramp time.
- The methods for evaluating $\tan\delta$, E', and E'' are valid for linear viscoelastic materials, meaning that the viscoelastic properties are independent of strain up to the limit of linear viscoelasticity. The limit of linear viscoelasticity reported for liver in literature is based on oscillatory shear experiments at different compressive preloads (Liu and Bilston, 2000; Tan et al., 2013; Wex et al., 2013; Ayyildiz et al., 2014). For example, Ayyildiz et al. (2014) found a linear shear strain limit of 1% at a prestrain of 5% for bovine liver. In the current study, DMA was performed at 8% prestrain, which was as low as possibly achievable with the given setup, while still avoiding compression of the sample throughout the whole test. Even though, the prestrain was higher than the limit for linear elasticity of 3% found in the ramp tests, the amplitude of oscillation (0.6%) was small enough to assume linear behaviour at the given prestrain level. However, we did not perform amplitude sweep experiments in tension to verify the linear viscoelastic limit.
- Given the long duration of the experiments (4 min for ramp tests, 5 min for relaxation, and 23 min for DMA), tissue dehydration cannot be ruled out completely. Wetting the samples during testing was not possible, as water drops on the point markers would have impeded the DIC measurement. Nicolle and Palierne (2010) found an increase in stiffness and damping behaviour due to dehydration in kidney tissue after a few minutes of dynamic shear testing.
- Furthermore, it should be noted that the tissue was not perfused, thus poroelastic behaviour was not modelled in the current study. According to (Kerdok et al., 2006) excised unperfused samples are stiffer and more viscous, compared to *in vivo* conditions.

6. Conclusion

Hepatic parenchyma tissue is non-linear and viscoelastic. Thus, for comprehensively describing liver mechanical properties, both aspects must be considered. First, the non-linear behaviour of porcine and bovine hepatic tissue was analysed via ramp tests and interpreted in the framework of a pseudoelastic Veronda-Westmann model for extracting strain-specific elastic moduli. Next, a method was presented to measure viscoelastic properties ($\tan\delta$, E'', and E'') in tension utilizing stress relaxation, as well as DMA. For each testing method, considerations about dissipated and stored energy were presented.

DMA is the gold standard for examining linear viscoelastic properties, but is associated with many experimental difficulties (e.g. the necessity of an extremely high temporal resolution of stress and strain measurement). We were able to answer the question whether loss tangent, storage modulus, and loss modulus, based on the relaxation experiments, could approximate the dynamic viscoelastic properties, affirmatively. However, special attention must be paid to the strain level at which the experiments are conducted when comparing the two methods, in order to avoid differing properties due to non-linearities.

The interesting discrepancies that were found regarding mechanical properties of bovine and porcine tissue call for further investigation on human hepatic tissue.

CRediT authorship contribution statement

Sarah-Jane Estermann: Methodology, Software, Formal analysis, Investigation, Visualization, Writing - original draft. **Dieter H. Pahr:** Resources, Funding acquisition, Project administration, Writing - reviewing & editing, Supervision. **Andreas Reisinger:** Conceptualization, Methodology, Validation, Data curation, Project administration, Writing - reviewing & editing, Supervision.

Declaration of competing interest

The authors declare that they have no known competing financial interests or personal relationships that could have appeared to influence the work reported in this paper.

Acknowledgements

The research was funded by the Niederösterreich Forschung & Bildung, Austria Science Call Dissertations 2017 (SC17-016), and the Austrian Center for Medical Innovation and Technology (funded in the framework of COMET by BMVIT, BMDW, the Federal State of Lower Austria and Standortagentur Tyrol). The authors acknowledge TU Wien University Library for financial support through its Open Access Funding Programme.

Table A.4
Overview of material models with corresponding true stress expressions and model parameters, and the corresponding coefficient of determination r^2 for a typical bovine hepatic sample.

Material model	Stress expression	Model parameters	r^2
Neo-Hookean	$\sigma_{NH} = 2\left(\lambda^2 - \frac{1}{\lambda}\right)c_1$	c_1	0.9054
Mooney–Rivlin	$\sigma_{MR} = 2\left(\lambda^2 - \frac{1}{\lambda}\right)\left(c_1 + c_2\frac{1}{\lambda}\right)$	c_1, c_2	0.9954
Veronda-Westmann	$\sigma_{VW} = 2\left(\lambda^2 - \frac{1}{\lambda}\right)c\beta\left(e^{\beta(I_1-3)} - \frac{1}{2\lambda}\right)$	c, β	0.9980
Yeoh	$\sigma_Y = 2\left(\lambda^2 - \frac{1}{\lambda}\right)(c_1 + 2c_2(I_1 - 3) + 3c_3(I_1 - 3)^2)$	c_1, c_2, c_3	0.9998

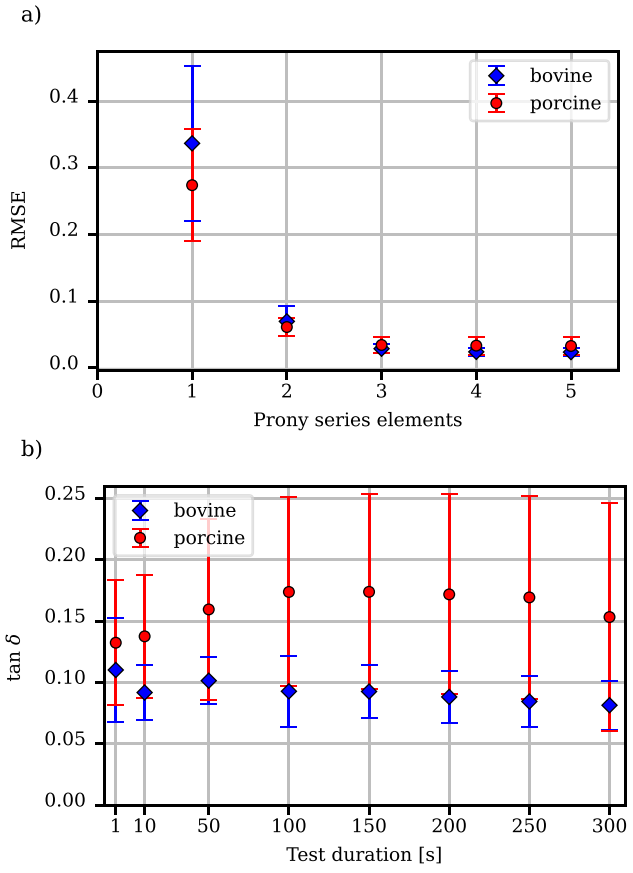

Fig. B.12. (a) The root-mean-square (RSME) and standard deviation of curve fitting Prony series with different numbers of elements to the 300 s of stress relaxation of bovine and porcine tissue ($f = 1$ Hz); (b) the loss tangent $\tan\delta$ plotted for varying relaxation durations ($N = 3$, $f = 1$ Hz).

Appendix A. Ramp test — Consideration of appropriate hyperelastic models

For selecting an appropriate hyperelastic model to represent the experimental ramp stress–stretch data, four different models varying in complexity were tested (Neo-Hookean, Mooney–Rivlin, Veronda-Westmann, and Yeoh). All four models have previously been used to describe hepatic tissue (Chui et al., 2004; Hollenstein et al., 2006; Umale et al., 2013). Table A.4 summarizes the models, applied in a hyperelastic framework for an isotropic, incompressible material under uniaxial tension with I_1 being the first strain invariant. The resulting stress–stretch curves for the different models and the experimental data are plotted in Fig. A.11 for a bovine hepatic sample during extension. The coefficients of determination ranged from $r^2 = 0.9054$ for the Neo-Hookean model to $r^2 = 0.9998$ for the Yeoh model (see Table A.4). The standard deviation of r^2 of each model was about 0.0005, when calculated for all samples in loading and unloading. Thus the curves depicted in Fig. A.11 are considered representative of the other samples.

The Yeoh model exhibited the highest coefficient of determination, however also has the largest number of fitting parameters. The Veronda-Westmann model also provided excellent correlation with the experimental data ($r^2 = 0.9980$) and has only two fitting parameters. Furthermore, the Veronda–Westmann model was originally developed specifically for soft tissues (Veronda and Westmann, 1970). Thus, the Veronda–Westmann model was chosen for further calculations.

Detailed description of the different models and derivations of the equations can be found elsewhere; for example in Holzapfel (2000) or Martins et al. (2006).

Appendix B. Stress relaxation — Influence of Prony series elements and holding time

Prony series elements. Concerning the choice of how many terms are necessary in Eq. (11) to accurately represent the experimental stress relaxation, the root-mean-square error (RMSE) – which describes the goodness of fit – was plotted for $N = \{1, 2, 3, 4, 5\}$ in Fig. B.12a. After reaching an average level of ~0.03 kPa for $N = 3$, the RMSE did not decrease significantly when the number of terms was increased to $N = \{4, 5\}$. Compared to $N = 3$, the RSME was about ten times higher for $N = 1$ and two times higher for $N = 2$. Thus, the three element Prony series approach was selected.

When fitting the Prony series to the experimental data, the duration of the holding time could influences the resulting viscoelastic properties. Thus, the loss tangent was examined by calculating $\tan\delta$ for cut-off times ranging from 10 to 300 s. The behaviour of $\tan\delta$ depending on changes in test duration, can be seen in Fig. B.12b. Even though the loss factors, calculated for different holding times, were statistically not distinguishable from each other, the influence of the finite ramp time may not be negligible for very short holding times (Liu and Bilston, 2002). For further investigation, $\tan\delta$ is reported for 300 s.

Appendix C. Supplementary data

Supplementary material related to this article can be found online at https://doi.org/10.1016/j.jmbbm.2020.104038.

References

Akhtar, R., Sherratt, M.J., Cruickshank, J.K., Derby, B., 2011. Characterizing the elastic properties of tissues. Mater. Today (Kidlington) 14 (3), 96–105. http://dx.doi.org/10.1016/s1369-7021(11)70059-1.

Alli, V.V., Yang, J., Xu, J., Bates, A.T., Pryor, A.D., Talamini, M.A., Telem, D.A., 2017. Nineteen-year trends in incidence and indications for laparoscopic cholecystectomy: the NY state experience. Surg. Endosc. 31 (4), 1651–1658. http://dx.doi.org/10.1007/s00464-016-5154-9.

Armijo, P.R., Pagkratis, S., Boilesen, E., Tanner, T., Oleynikov, D., 2018. Growth in robotic-assisted procedures is from conversion of laparoscopic procedures and not from open surgeons' conversion: a study of trends and costs. Surg. Endosc. 32, 2106–2113. http://dx.doi.org/10.1007/s00464-017-5908-z.

Ayyildiz, M., Aktas, R., Basdogan, C., 2014. Effect of solution and post-mortem time on mechanical and histological properties of liver during cold preservation. Biorheology 51, http://dx.doi.org/10.3233/bir-14007.

Bartolini, L., Iannuzzi, D., Mattei, G., 2018. Comparison of frequency and strain-rate domain mechanical characterization. Sci. Rep. 8 (1), 13697. http://dx.doi.org/10.1038/s41598-018-31737-3.

Brunon, A., Bruyère-Garnier, K., Coret, M., 2010. Mechanical characterization of liver capsule through uniaxial quasi-static tensile tests until failure. J. Biomech. 43 (11), 2221–2227. http://dx.doi.org/10.1016/j.jbiomech.2010.03.038.

Capilnasiu, A., Bilston, L., Sinkus, R., Nordsletten, D., 2020. Nonlinear viscoelastic constitutive model for bovine liver tissue. Biomech. Model. Mechanobiol. http://dx.doi.org/10.1007/s10237-020-01297-5.

Chatelin, S., Oudry, J., Perichon, N., Sandrin, L., Allemann, P., Soler, L., Willinger, R., 2011. In vivo liver tissue mechanical properties by transient elastography: comparison with dynamic mechanical analysis. Biorheology 48, 75–88. http://dx.doi.org/10.3233/bir-2011-0584.

Chen, X., Masano, N., Teppei, T., Xin, J., Satoko, A., Koyu, A., Atsushi, K., Masaru, U., 2011. Identification of physical properties of swine liver for surgical simulation using a dynamic deformation model. System Integration (SII), 2011 IEEE/SICE International Symposium on 655–660. http://dx.doi.org/10.1109/sii.2011.6147526.

Chen, E.J., Novakofski, J., Jenkins, W.K., O'Brien, W.D., 1996. Young's modulus measurements of soft tissues with application to elasticity imaging. IEEE Trans. Ultrason. Ferroelectr. Freq. Control 43 (1), 191–194. http://dx.doi.org/10.1109/58.484478.

Chen, R., Rodrigues Armijo, P., Krause, C., Siu, K.-C., Oleynikov, D., 2020. A comprehensive review of robotic surgery curriculum and training for residents, fellows, and postgraduate surgical education. Surg. Endosc. 34 (1), 361–367. http://dx.doi.org/10.1007/s00464-019-06775-1.

Chui, C., Kobayashi, E., Chen, X., Hisada, T., Sakuma, I., 2004. Combined compression and elongation experiments and non-linear modelling of liver tissue for surgical simulation. Med. Biol. Eng. Comput. 42 (6), 787–798. http://dx.doi.org/10.1007/bf02345212.

DeWall, R.J., Bharat, S., Varghese, T., Hanson, M.E., Agni, R.M., Kliewer, M.A., 2012. Characterizing the compression-dependent viscoelastic properties of human hepatic pathologies using dynamic compression testing. Phys. Med. Biol. 57 (8), 2273–2286. http://dx.doi.org/10.1088/0031-9155/57/8/2273.

Dunford, K.M., LeRoith, T., Kemper, A.R., 2018. Effects of postmortem time and storage fluid on the material properties of bovine liver parenchyma in tension. J. Mech. Behav. Biomed. Mater. 87, 240–255. http://dx.doi.org/10.1016/j.jmbbm.2018.05.043.

Duong, M.T., Nguyen, N.H., Tran, T.N., Tolba, R.H., Staat, M., 2015. Influence of refrigerated storage on tensile mechanical properties of porcine liver and spleen. Int. Biomech. 2 (1), 79–88. http://dx.doi.org/10.1080/23335432.2015.1049295.

Estermann, S.-J., Pahr, D.H., Reisinger, A., 2020. Quantifying tactile properties of liver tissue, silicone elastomers, and a 3D printed polymer for manufacturing realistic organ models. J. Mech. Behav. Biomed. Mater. 104, 103630. http://dx.doi.org/10.1016/j.jmbbm.2020.103630.

Eurell, J., Frappier, B., 2006. Dellmann's Textbook of Veterinary Histology. Blackwell Publishing, Ames.

Findley, W.N., Lai, J.S., Onaran, K., 1989. Creep and Relaxation of Nonlinear Viscoelastic Materials. Dover Publications, Inc., New York.

Fung, Y.C., 1967. Elasticity of soft tissues in simple elongation. Am. J. Physiol. 213 (6), 1532–1544. http://dx.doi.org/10.1152/ajplegacy.1967.213.6.1532.

Fung, Y.C., 1993. Biomechanics: Mechanical Properties of Living Tissues, second ed. Springer Science+Business Media New York, http://dx.doi.org/10.1007/978-1-4757-2257-4.

Gao, Z., Lister, K., Desai, J.P., 2010. Constitutive modeling of liver tissue: Experiment and theory. Ann. Biomed. Eng. 38 (2), 505–516. http://dx.doi.org/10.1007/s10439-009-9812-0.

Gutierrez-Lemini, D., 2014. Engineering Viscoelasticity. Springer, New York, http://dx.doi.org/10.1007/978-1-4614-8139-3.

Hata, S., Imamura, H., Aoki, T., Hashimoto, T., Akahane, M., Hasegawa, K., Bekku, Y., Sugawara, Y., Makuuchi, M., Kokudo, N., 2011. Value of visual inspection, bimanual palpation, and intraoperative ultrasonography during hepatic resection for liver metastases of colorectal carcinoma. World J. Surg. 35 (12), 2779–2787. http://dx.doi.org/10.1007/s00268-011-1264-7.

Hildebrand, P., Kleemann, M., Roblick, U., Mirow, L., Bruch, H.-P., Bürk, C., 2007. Development of a perfused ex vivo tumor-mimic model for the training of laparoscopic radiofrequency ablation. Surg. Endosc. 21 (10), 1745–1749. http://dx.doi.org/10.1007/s00464-007-9216-x.

Hollenstein, M., Nava, A., Valtorta, D., Snedeker, J., Mazza, E., 2006. Mechanical characterization of the liver capsule and parenchyma. In: Harders, M., Szekely, G. (Eds.), In: Lecture Notes in Computer Science, vol. 4072, Springer, Berlin, Heidelberg, pp. 150–158,

Holzapfel, G.A., 2000. Nonlinear Solid Mechanics. John Wiley and Sons, New York.

Jing, Y., Lingtao, Y., Wang, L., Hongyang, L., An, Q., 2016. Study on mechanical characterization of liver tissue based on haptic devices for virtual surgical simulation. J. Mech. Med. Biol. 16 (8), 1640016. http://dx.doi.org/10.1142/s0219519416400169.

Kanta, J., 2016. Elastin in the liver. Front. Physiol. 7, 491. http://dx.doi.org/10.3389/fphys.2016.00491.

Karimi, A., Shojaei, A., 2018. An experimental study to measure the mechanical properties of the human liver. Dig. Dis. 36, 150–155. http://dx.doi.org/10.1159/000481344.

Kemper, A.R., Santago, A.C., Stitzel, J.D., Sparks, J.L., Duma, S.M., 2010. Biomechanical response of human liver in tensile loading. Ann. Adv. Automot. Med. 54, 15–26, URL: http://www.ncbi.nlm.nih.gov/pmc/articles/PMC3242546/.

Kerdok, A.E., Ottensmeyer, M.P., Howe, R.D., 2006. Effects of perfusion on the viscoelastic characteristics of liver. J. Biomech. 39 (12), 2221–2231. http://dx.doi.org/10.1016/j.jbiomech.2005.07.005.

Kiss, M.Z., Varghese, T., Hall, T.J., 2004. Viscoelastic characterization of in vitro canine tissue. Phys. Med. Biol. 49 (18), 4207–4218. http://dx.doi.org/10.1088/0031-9155/49/18/002.

Laird, A., Stewart, G.D., Hou, S., Tang, B., McLornan, M.E., Riddick, A.C.P., McNeill, S.A., 2011. A novel bovine model for training urological surgeons in laparoscopic radical nephrectomy. J. Endourol. 25 (8), 1377–1383. http://dx.doi.org/10.1089/end.2011.0060.

Lim, Y.-J., Deo, D., Singh, T.P., Jones, D.B., De, S., 2009. In situ measurement and modeling of biomechanical response of human cadaveric soft tissues for physics-based surgical simulation. 2008/09/24 Surg. Endosc. 23 (6), 1298–1307. http://dx.doi.org/10.1007/s00464-008-0154-z.

Limbert, G. (Ed.), 2019. Skin Biophysics: From Experimental Characterisation to Advanced Modelling. Springer, Cham, Switzerland, http://dx.doi.org/10.1007/978-3-030-13279-8.

Liu, Z., Bilston, L., 2000. On the viscoelastic character of liver tissue: Experiments and modelling of the linear behaviour. Biorheology 37, 191–201.

Liu, Z., Bilston, L., 2002. Large deformation shear properties of liver tissue. Biorheology 39, 735–742.

Liu, W., Zheng, X., Wu, R., Jin, Y., Kong, S., Li, J., Lu, J., Yang, H., Xu, X., Lv, Y., Zhang, X., 2018. Novel laparoscopic training system with continuously perfused ex-vivo porcine liver for hepatobiliary surgery. Surg. Endosc. 32 (2), 743–750. http://dx.doi.org/10.1007/s00464-017-5731-6.

Lowe, J.S., Anderson, P.G., 2015. Stevens & Lowe's Human Histology. Mosby, Philadelphia.

Lu, Y.-C., Kemper, A.R., Untaroiu, C.D., 2014. Effect of storage on tensile material properties of bovine liver. J. Mech. Behav. Biomed. Mater. 29, 339–349. http://dx.doi.org/10.1016/j.jmbbm.2013.09.022.

Manoogian, S.J., Bisplinghoff, J.A., McNally, C., Kemper, A.R., Santago, A.C., Duma, S.M., 2009. Effect of strain rate on the tensile material properties of human placenta. J. Biomech. Eng. 131 (9), http://dx.doi.org/10.1115/1.3194694, 091008–091006.

Marchesseau, S., Chatelin, S., Delingette, H., 2017. Nonlinear biomechanical model of the liver: Hyperelastic constitutive laws for finite element modeling. In: Payan, Y., Ohayon, J. (Eds.), Biomechanics of Living Organs. Aca. Press, Elsevier, pp. 243–265. http://dx.doi.org/10.1016/B978-0-12-804009-6.00011-0.

Marquardt, D., 1963. An algorithm for least-squares estimation of nonlinear parameters. SIAM J. Appl. Math. 11 (2), 431–441. http://dx.doi.org/10.1137/0111030.

Martins, P.A.L.S., Natal Jorge, R., Ferreira, A., 2006. A comparative study of several material models for prediction of hyperelastic properties: Application to silicone-rubber and soft tissues. Strain 42 (3), 135–147. http://dx.doi.org/10.1111/j.1475-1305.2006.00257.x.

Mattice, J.M., Lau, A.G., Oyen, M.L., Kent, R.W., 2006. Spherical indentation load-relaxation of soft biological tissues. J. Mater. Res. 21, http://dx.doi.org/10.1557/jmr.2006.0243.

Miller, K., Chinzei, K., 1997. Constitutive modelling of brain tissue: Experiment and theory. J. Biomech. 30 (11), 1115–1121. http://dx.doi.org/10.1016/S0021-9290(97)00092-4.

Neuman, R.E., Logan, M.A., 1950. The determination of collagen and elastin in tissues. J. Biol. Chem. 186 (2), 549–556.

Nicolle, S., Palierne, J.-F., 2010. Dehydration effect on the mechanical behaviour of biological soft tissues: Observations on kidney tissues. J. Mech. Behav. Biomed. Mater. 3 (8), 630–635. http://dx.doi.org/10.1016/j.jmbbm.2010.07.010.

Nicolle, S., Vezin, P., Palierne, J.-F., 2010. A strain-hardening bi-power law for the nonlinear behaviour of biological soft tissues. J. Biomech. 43 (5), 927–932. http://dx.doi.org/10.1016/j.jbiomech.2009.11.002.

Ocal, S., Umut Ozcan, M., Basdogan, I., Basdogan, C., 2010. Effect of preservation period on the viscoelastic material properties of soft tissues with implications for liver transplantation. J. Biomech. Eng. 132, 101007. http://dx.doi.org/10.1115/1.4002489.

Oyen, M., 2005. Spherical indentation creep following ramp loading. J. Mater. Res. 20, http://dx.doi.org/10.1557/jmr.2005.0259.

Roan, E., Vemaganti, K., 2011. Strain rate-dependent viscohyperelastic constitutive modeling of bovine liver tissue. Med. Biol. Eng. Comput. 49 (4), 497–506. http://dx.doi.org/10.1007/s11517-010-0702-2.

Roylance, D., 2001. Engineering Viscoelasticity. Massachusetts Institute of Technology: MIT OpenCourseWare, URL: https://ocw.mit.edu/.

Santago, A.C., Kemper, A.R., McNally, C., Sparks, J., Duma, S.M., 2009. The effect of temperature on the mechanical properties of bovine liver. Biomed. Sci. Instrum. 45, 376–381.

Shergold, O.A., Fleck, N.A., Radford, D., 2006. The uniaxial stress versus strain response of pig skin and silicone rubber at low and high strain rates. Int. J. Impact Eng. 32 (9), 1384–1402. http://dx.doi.org/10.1016/j.ijimpeng.2004.11.010.

Snedeker, J., Niederer, P., Schmidlin, F., Farshad, M., Demetropoulos, C., Lee, J., Yang, K., 2005. Strain-rate dependent material properties of the porcine and human kidney capsule. J. Biomech. 38, 1011–1021. http://dx.doi.org/10.1016/j.jbiomech.2004.05.036.

Tamura, A., Omori, K., Miki, K., Lee, J.B., Yang, K.H., King, A.I., 2002. Material characterization of porcine abdominal organs. Stapp Car Crash J. 46, 55–69.

Tan, K., Cheng, S., Jugé, L., Bilston, L., 2013. Characterising soft tissues under large amplitude oscillatory shear and combined loading. J. Biomech. 46 (6), 1060–1066. http://dx.doi.org/10.1016/j.jbiomech.2013.01.028.

Taylor, L., Lerner, A., Rubens, D., Parker, K., 2002. A Kelvin-Voight fractional derivative model for viscoelastic characterization of liver tissue. In: Proceedings of IMECE2002 ASME International Mechanical Engineering Congress & Exposition, vol. 53. http://dx.doi.org/10.1115/imece2002-32605.

Uehara, H., 1995. A study on the mechanical properties of the kidney, liver, and spleen, by means of tensile stress test with variable strain velocity. J. Kyoto Prefectural Univ. Med. 104 (1), 439–451.

Umale, S., Deck, C., Bourdet, N., Dhumane, P., Soler, L., Marescaux, J., Willinger, R., 2013. Experimental mechanical characterization of abdominal organs: liver, kidney & spleen. J. Mech. Behav. Biomed. Mater. 17, 22–33. http://dx.doi.org/10.1016/j.jmbbm.2012.07.010.

Veronda, D.R., Westmann, R.A., 1970. Mechanical characterization of skin–finite deformations. J. Biomech. 3 (1), 111–124. http://dx.doi.org/10.1016/0021-9290(70)90055-2.

Wex, C., Stoll, A., Fröhlich, M., Arndt, S., Lippert, H., 2013. How preservation time changes the linear viscoelastic properties of porcine liver. Biorheology 50, 115–131. http://dx.doi.org/10.3233/BIR-130632.

Wex, C., Stoll, A., Fröhlich, M., Arndt, S., Lippert, H., 2014. Mechanics of fresh, frozen-thawed and heated porcine liver tissue. Int. J. Hyperthermia 30 (4), 271–283. http://dx.doi.org/10.3109/02656736.2014.924161.

Yoganandan, N., Pintar, F.A., Gennarelli, T.A., Maltese, M.R., 2000. Patterns of abdominal injuries in frontal and side impacts. Annu. Proc. Assoc. Adv. Automot. Med. 44 (11558081), 17–36, URL: https://www.ncbi.nlm.nih.gov/pmc/articles/PMC3217390/.

Yoshida, H., Taniai, N., Yoshioka, M., Hirakata, A., Kawano, Y., Shimizu, T., Ueda, J., Takata, H., Nakamura, Y., Mamada, Y., 2019. Current status of laparoscopic hepatectomy. J. Nippon Med. Sch. 86 (4), 201–206. http://dx.doi.org/10.1272/jnms.jnms.2019_86-411.

Zhang, S., 1999. An Atlas of Histology. Sprinnger-Verlag, New York.

Zhang, M., Castaneda, B., Wu, Z., Nigwekar, P., Joseph, J.V., Rubens, D.J., Parker, K.J., 2007. Congruence of imaging estimators and mechanical measurements of viscoelastic properties of soft tissues. Ultrasound Med. Biol. 33 (10), 1617–1631. http://dx.doi.org/10.1016/j.ultrasmedbio.2007.04.012.

Zhang, X., Gao, X., Zhang, P., Guo, Y., Lin, H., Diao, X., Liu, Y., Dong, C., Hu, Y., Chen, S., Chen, X., 2017. Dynamic mechanical analysis to assess viscoelasticity of liver tissue in a rat model of nonalcoholic fatty liver disease. Med. Eng. Phys. 44, 79–86. http://dx.doi.org/10.1016/j.medengphy.2017.02.014.

Zhu, Y., Zheng, Y., Shen, Y.-Y., Chen, X., Zhang, X.-Y., Lin, H.-M., Guo, Y.-R., Wang, T.-R., Chen, S.-P., 2013. Analyzing and modeling rheological behavior of liver fibrosis in rats using shear viscoelastic moduli. J. Zhejiang Univ. Sci. B 15 (4), 375–381. http://dx.doi.org/10.1631/jzus.b1300121.